



Adsorption mechanism of styryl phosphonate ester as collector in ilmenite flotation

Yan-ling XU¹, Kai-hua HUANG², Hong-qiang LI³, Wei HUANG⁴, Cheng LIU¹, Si-yuan YANG^{1,3}

1. School of Resources and Environmental Engineering, Wuhan University of Technology, Wuhan 430070, China;
2. South China Institute of Environmental Sciences, Ministry of Ecology and Environment, Guangzhou 510530, China;
3. Engineering Research Center of Phosphorus Resources Development and Utilization of Ministry of Education, Wuhan Institute of Technology, Wuhan 430205, China;
4. Academy for Advanced Interdisciplinary Studies, Southern University of Science and Technology, Shenzhen 518055, China

Received 6 September 2021; accepted 26 April 2022

Abstract: A styryl phosphonate ester (SPE) collector was used to improve the flotation performance of ilmenite, and the adsorption mechanism and model were revealed and established, respectively. Microflotation tests showed that SPE exhibited a stronger collecting ability for ilmenite than the traditional collector styrene phosphonic acid (SPA). Zeta potential measurements revealed that both SPE and SPA could negatively shift the zeta potential of ilmenite, while SPE had more effects than SPA, suggesting the stronger adsorption of SPE. The analysis of X-ray photoelectron spectroscopy confirmed the chemisorption of SPA and SPE onto the Fe/Ti sites of ilmenite. According to frontier orbital theory, the chemical activities of SPE are greater than those of SPA. The partial densities of states analysis indicated that the PO—H groups of the collectors could interact with the Ti/Fe atoms of the ilmenite surface to generate a stable four-membered ring. The bonding model of the collector and (104) ilmenite surface showed that the adsorption energy of SPE was higher than that of SPA. Overall, SPE presented a better collecting ability and interaction effect for ilmenite flotation than SPA, and had the potential to replace SPA in the industry.

Key words: styryl phosphonate ester; ilmenite; flotation; collector; X-ray photoelectron spectroscopy; density functional theory; adsorption mechanism

1 Introduction

Titanium has been widely used in military, aerospace, automobile, and refractory materials due to its excellent physical and chemical properties, such as low density, high strength and melting point, good elasticity, and corrosion resistance [1–4]. The main mineral sources of titanium are ilmenite, rutile and anatase, in which ilmenite occupies 90% of the total titanium primary resources worldwide [5]. In China, ilmenite is mainly found in vanadium–titanium magnetite in Panzhihua,

Sichuan Province, China [5,6].

Ilmenite can be separated from gangue minerals (quartz, titanite, pyroxene, etc.) based on the differences in their physical properties through methods such as magnetic separation [7], gravity separation [8] and electrical separation [9]. Nonetheless, froth flotation is considered the most effective method for upgrading fine ilmenite ore, and proper selection of reagent schemes (collector and regulator) is extremely important [10]. Several collectors have been applied in ilmenite flotation, including sodium oleate (NaOl), benzohydroxamic acid (BHA) [11] and styrene phosphonic acid

Corresponding author: Si-yuan YANG, Tel: +86-13294166556, E-mail: siyuan.yang@whut.edu.cn;
Cheng LIU, Tel: +86-15827073630, E-mail: liucheng309@whut.edu.cn

DOI: 10.1016/S1003-6326(22)66080-1

1003-6326/© 2022 The Nonferrous Metals Society of China. Published by Elsevier Ltd & Science Press

(SPA) [12,13], but challenges still remain in achieving satisfactory flotation performance.

NaOl is a common collector with a low price and a wide source; however, its selectivity is poor when employed in the flotation separation of ilmenite from silicated gangue minerals [6]. BHA has been proven to be an efficient collector of ilmenite using flotation means and exhibits superior selectivity against quartz and titanite [14,15]. However, BHA often requires a large consumption concentration or the extra usage of an activator due to its weak collecting ability [16–18]. SPA was first introduced in cassiterite flotation and became popular in ilmenite flotation due to its strong selectivity for silicate gangue minerals [12,19]; however, it also requires a high concentration and an additional frother. Thus, a novel collector for ilmenite flotation is needed. Modifying or introducing functional groups of molecules to develop more efficient collectors has become an important method of improving the flotation performance of ilmenite [20,21].

SPA has exhibited good flotation performance and has been widely applied in the flotation of metal oxide minerals [21]. Nevertheless, the collecting ability of SPA is relatively poor, and its industrial application requires a high collector concentration and a frother, leading to environmental issues and high economic costs. It has been proven that the modification of the molecular structure is an effective way to improve the flotation performance of collectors [22]. Therefore, we hope to enhance the collecting ability of SPA by introducing an ester group into its molecule. In this study, styryl phosphonate ester (SPE) was synthesized by introducing an ester group into the SPA molecule to improve its hydrophobicity and flotation performance [23]. SPE was introduced as a collector for ilmenite flotation. Using the novel surfactant of SPE containing an ester group is an interesting means to improve ilmenite floatability that deserves further investigation. The hydrophobization mechanism can be deeply explored through comparison with a single-polar-group collector, which is instructive in developing new flotation reagents [24]. The ability of SPE to collect ilmenite for flotation was evaluated by microflotation tests. In addition, the adsorption mechanism of SPE onto the ilmenite surface was revealed by zeta potential measurements, X-ray

photoelectron spectroscopy (XPS) analysis and density functional theory (DFT) modeling.

2 Experimental

2.1 Materials and reagents

The ilmenite sample used in this study was purchased from Panzhihua, China. The XRD pattern in Fig. 1 showed only ilmenite in this sample. The X-ray fluorescence (XRF) [25] results confirmed the high purity of ilmenite with 48.66 wt.% TiO_2 , as revealed in Table 1. The ilmenite sample was ground to a size fraction of 38–74 μm by ball milling for use in microflotation tests.

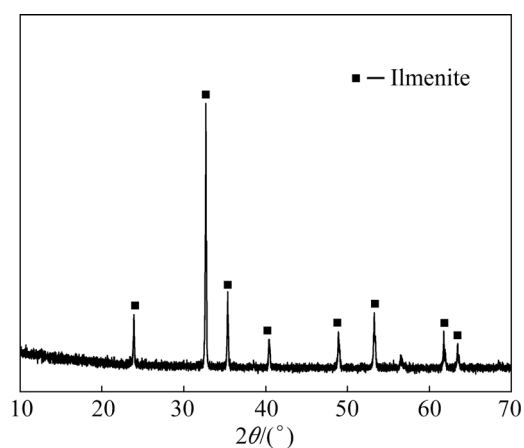


Fig. 1 XRD pattern of ilmenite sample

Table 1 Main chemical compositions of ilmenite sample (mass fraction, %)

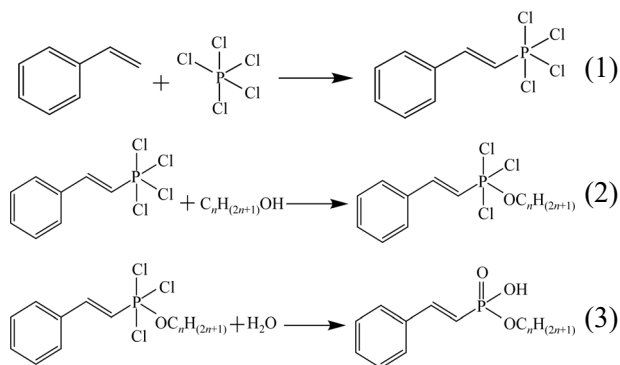
TiO_2	Fe_2O_3	MgO	SiO_2	CaO	MnO	Al_2O_3
48.66	44.45	3.84	1.01	0.42	0.64	0.62

Chemical-grade of frother terpenic oil and collector SPA were purchased from Sinopharm Chemical Reagent Co., Ltd. The SPE with a grade >98% was synthesized and purified in our laboratory. Deionized water with a resistivity of 18.2 $\text{m}\Omega\cdot\text{cm}$ was used for all the experimental tests in this study.

2.2 Synthesis procedure of SPE

SPE was synthesized using phosphorus pentachloride and styrene as raw materials. The intermediate (styrene phosphine tetrachloride) was firstly synthesized by Reaction (1), and then reacted with alcohol and water in sequence as shown in

Reactions (2) and (3). The optimal synthesis conditions are listed as follows: chloroform was used as the solvent; the molar ratio of styrene: phosphorus pentachloride : *n*-butanol was set to be 1:1.2:1.5; the reaction time of the first, second and third steps is 4, 2 and 1 h, respectively, with the reaction temperature of 50 °C. The characterization of SPE is shown in Figs. S1–S4 in Supplementary Materials, confirming the successful synthesis of high-purity SPE.



2.3 Microflotation tests

A mechanically agitated flotation machine [26] with a fixed impeller speed of 1800 r/min was used for the microflotation tests. A total of 3.0 g of 38–74 μm mineral and 40 mL of deionized water were successively added to a plexiglass flotation cell. The slurry was adjusted to the desired pH value with dilute NaOH or H₂SO₄ solutions, and the required concentrations of collector and frother were added sequentially with a conditioning time of 3 min. The suspension pH was recorded before turning on the air supply, and flotation was conducted for 5 min. The float and sink products were collected and weighed to calculate the recovery. Each test was performed twice, and the average value was reported with standard deviations presented as the error bars.

2.4 Zeta potential measurement

The zeta potentials of minerals were measured with a Zetasizer Nano ZS90 instrument (Malvern Instruments, England). Ilmenite samples were freshly ground to a size of <2 μm using an agate mortar. The suspension was prepared by adding 30 mg of ilmenite to 20 mL of 1 mmol/L electrolyte [27], which was magnetically stirred for 20 min in a beaker according to the required reagent scheme. Afterward, the suspension was allowed to settle for 10 min, and the supernatant was collected

and injected into a sample cell for zeta potential measurements. The error bars in each plot represent one standard deviation of uncertainty obtained from three independent runs.

2.5 XPS analysis

The XPS spectra of ilmenite before and after treatment with SPA or SPE were measured with an Al K_α 1063 spectrometer (Thermo Fisher Scientific, USA), under the operating conditions of 200 W power, an Al K_α X-ray source and 20 eV pass energy. Thermo Avantage software was utilized to conduct the peak fitting of the XPS spectra. The testing sample was prepared by mixing 2.0 g of ilmenite (<2 μm) with 50 mL of the 25 mg/L collector at pH 6.0. Afterward, Milli-Q water was used to filter and wash the suspension twice to remove the physical adsorption of the collector. Finally, the filtered minerals were dried in a vacuum drying oven before being subjected to XPS analysis.

2.6 DFT calculation

DFT calculations were completed by the Dmol³ and CASTEP modules using Material Studio 2017 software. The CASTEP module was applied to establishing plane and crystal models [28], while the Dmol³ module was used to analyze the frontier orbital energy [21]. In addition, the establishment and optimization of the collector adsorption model onto the ilmenite surface and the related calculations were performed in the CASTEP module.

A periodic model of ilmenite bulk phases using XRD crystal structures was obtained from the American Mineralogical Crystal Structure Database [29]. The optimized supercell (2 × 2 × 1) of the ilmenite bulk structure was used to generate a surface slab model that crossed a specified crystal plane (104) [30]. The (104) surface plate model with a vacuum zone of 40 Å was optimized for calculating the vacuum adsorption energy. DFT calculations within the GGA-PW91 functionality were conducted to study the collector adsorption onto the ilmenite surfaces. The kinetic energy cutoff, *k*-points and pseudopotential were set to 500.0 eV, 6×6×2 and ultrasoft, respectively [14]. The energy of the lowest unoccupied molecule orbit (*E*_{LUMO}) and energy of the highest occupied molecule orbit (*E*_{HOMO}) of the collectors were calculated using the

DMol³ module with functional B3LYP and basis DNP. The models of the ilmenite crystal and molecular structures of the collectors (SPA and SPE) were geometrically optimized, as shown in Fig. 2.

The adsorption energy, E_{ads} , of the collectors on the ilmenite surface can be calculated as follows [7,31]:

$$E_{\text{ads}} = E_{\text{surf/dep}} - E_{\text{surf}} - E_{\text{dep}} \quad (4)$$

where E_{surf} and $E_{\text{surf/dep}}$ are the total energy of the ilmenite slab before and after collector adsorption, respectively, and E_{dep} is the total energy of the free collector molecules.

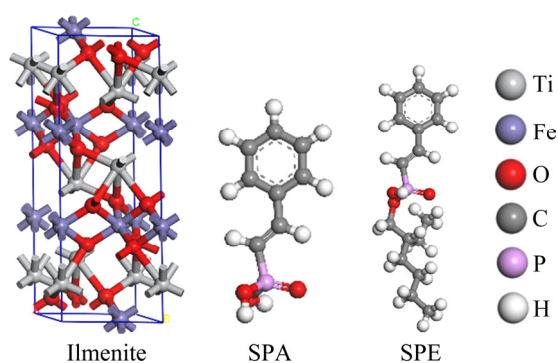


Fig. 2 Molecular structures of ilmenite, SPA, and SPE

3 Results and discussion

3.1 Microflotation performance of ilmenite using SPE

To evaluate the collecting ability of SPE and SPA for ilmenite flotation, microflotation tests were conducted under different pH values and collector concentrations. Figure 3 shows the ilmenite floatability as a function of pulp pH in the presence of 25 mg/L collector and 0.1 mg/L terpenic oil. This result reveals that ilmenite flotation recovery presented a similar trend using either SPE or SPA as the collector, which increased at pH 2.0–6.0 while reducing from pH 6.0 to pH 12.0. Specifically, at pH 6.0, SPA could only obtain 70.4% ilmenite flotation recovery, while the novel collector SPE led to a much higher recovery of 99%, suggesting that SPE had a much stronger collecting ability than SPA.

The effects of collector concentration on ilmenite flotation recovery at pH 6.0 are shown in Fig. 4. The flotation recovery of ilmenite increased rapidly with increasing concentrations of SPA or SPE. The ilmenite recovery reached 99.0% at

25 mg/L SPA and remained nearly unchanged when the collector concentration continued to increase. On the other hand, SPA could only achieve satisfying ilmenite flotation performance under a high reagent concentration of >150 mg/L. Hence, the microflotation test results reveal that SPE has a superior ability to collect ilmenite during flotation compared with SPA.

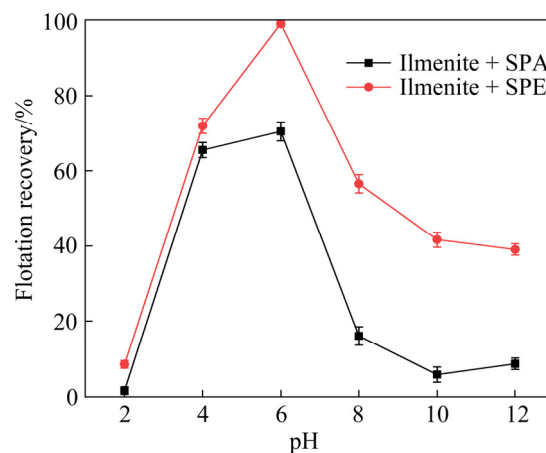


Fig. 3 Flotation recovery of ilmenite as function of pH using collector (Flotation conditions: 25 mg/L collector; 0.1 mg/L terpenic oil)

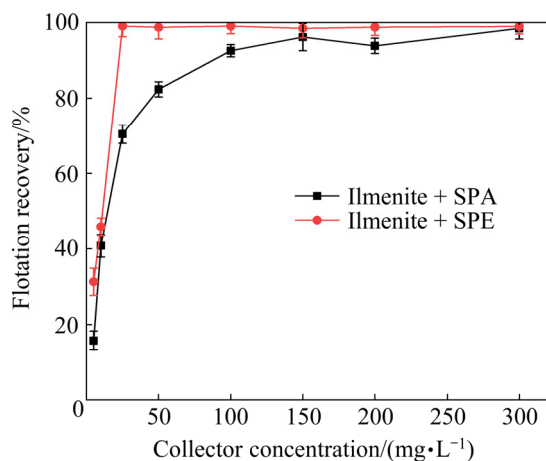


Fig. 4 Flotation recovery of ilmenite as function of collector concentration (Flotation conditions: pH=6.0; 0.1 mg/L terpenic oil)

3.2 Zeta potential measurement results

To investigate the adsorption mechanism of SPE onto the ilmenite surface, zeta potential measurements of ilmenite in the absence and presence of a collector were performed as a pH function, and the results are plotted in Fig. 5. As shown, the isoelectric point (IEP) of ilmenite was located at pH ~4.6, which is consistent with previous studies [32,33]. The ilmenite surface

groups were primarily Ti^{4+} , FeOH^+ , $\text{Ti}(\text{OH})^{3+}$, $\text{Ti}(\text{OH})_2^{2+}$, and $\text{Ti}(\text{OH})^{3+}$ under acidic conditions. Thus, the zeta potential will be positive in strongly acidic solutions. With increasing pH values, the zeta potential of ilmenite moved in a negative direction and eventually became negative due to the higher hydroxylation degree of the ilmenite surface [2,8]. After the addition of the collector, the zeta potential of ilmenite negatively moved throughout the whole studied pH range. SPE presented a greater effect on the zeta potential of ilmenite than SPA in the pH range of 2.0–10.0, indicating that SPE was adsorbed more strongly onto the ilmenite surface.

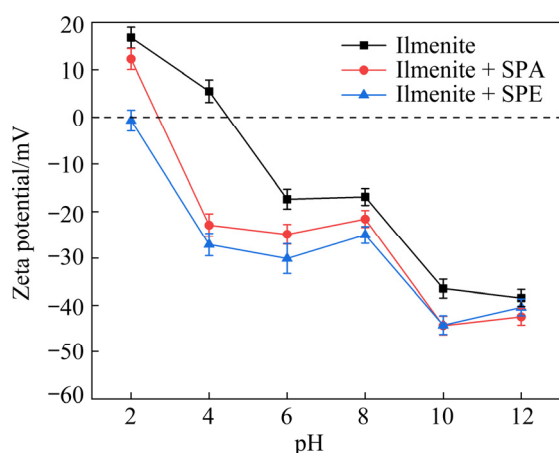


Fig. 5 Zeta potentials of ilmenite as function of pH in the presence of different collectors (Condition: 25 mg/L collector)

3.3 XPS spectra of ilmenite with collectors

The changes in the chemical states and elemental compositions on ilmenite surfaces with or without the collector addition were investigated by XPS analysis. Thermo Avantage software was used for the peak fitting of the XPS spectra. The “Smart” option was chosen for the background line fitting, the default value of 0.3 was used for the Lorentzian–Gaussian (L/G) ratio, the FWHM range of the main peak was 0.3–1.7 eV, and the double peak area ratio of $2p_{1/2}$ to $2p_{3/2}$ being 1:2 was selected for Ti and Fe. Figure 6(a) shows that the Ti 2p spectra of raw ilmenite can be fitted by four characteristic peaks, where the peak at 458.2 eV was attributed to Ti^{4+} of Ti—O—Fe [34–36]; the peak at 459.6 eV referred to Ti^{4+*} of the TiO_2 rutile (110) surface [37,38]; the peaks at 463.8 and 465.1 eV corresponded to the spin-orbital splitting photoelectrons of ilmenite. After ilmenite was treated with SPA, as shown in Fig. 6(b), the binding energies of Ti^{4+} and Ti^{4+*} were

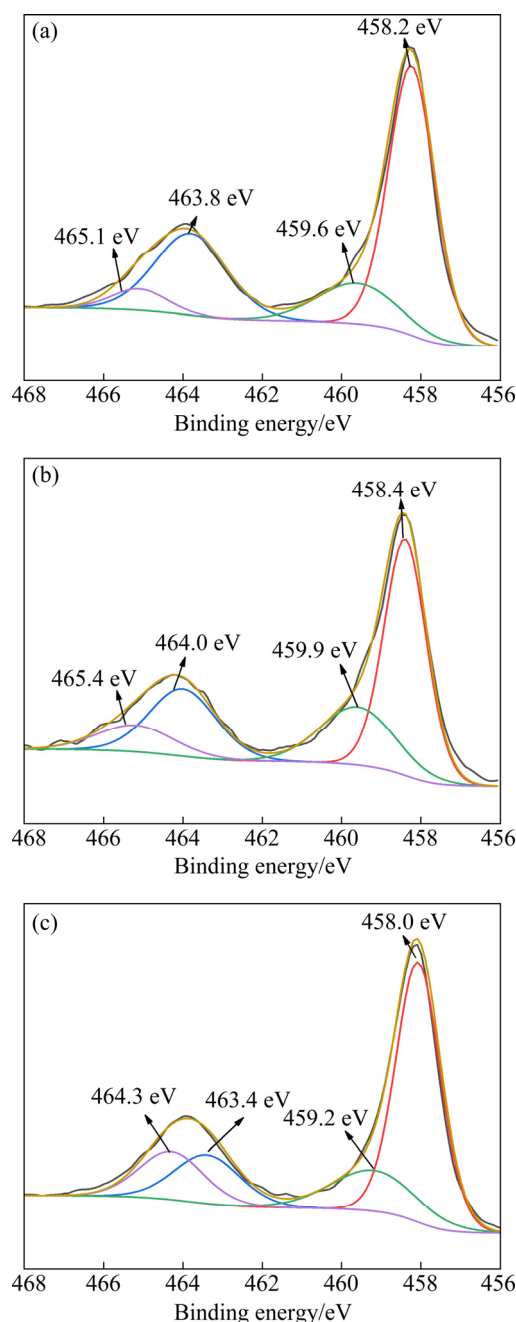


Fig. 6 XPS spectra of Ti 2p on surfaces of bare (a), SPA-treated (b) and SPE-treated (c) ilmenite

shifted by 0.2 and 0.3 eV, respectively, indicating a chemical reaction between SPA and Ti on the ilmenite surface. Figure 6(c) reveals that the binding energies of each peak of Ti 2p of ilmenite were changed by 0.2 and 0.4 eV after SPE treatment, indicating that SPE had stronger chemisorption onto the Ti sites of the ilmenite surface.

Figure 7 shows the Fe 2p spectra of ilmenite before and after collector treatment. As shown in Fig. 7(a), the XPS spectrum of bare ilmenite

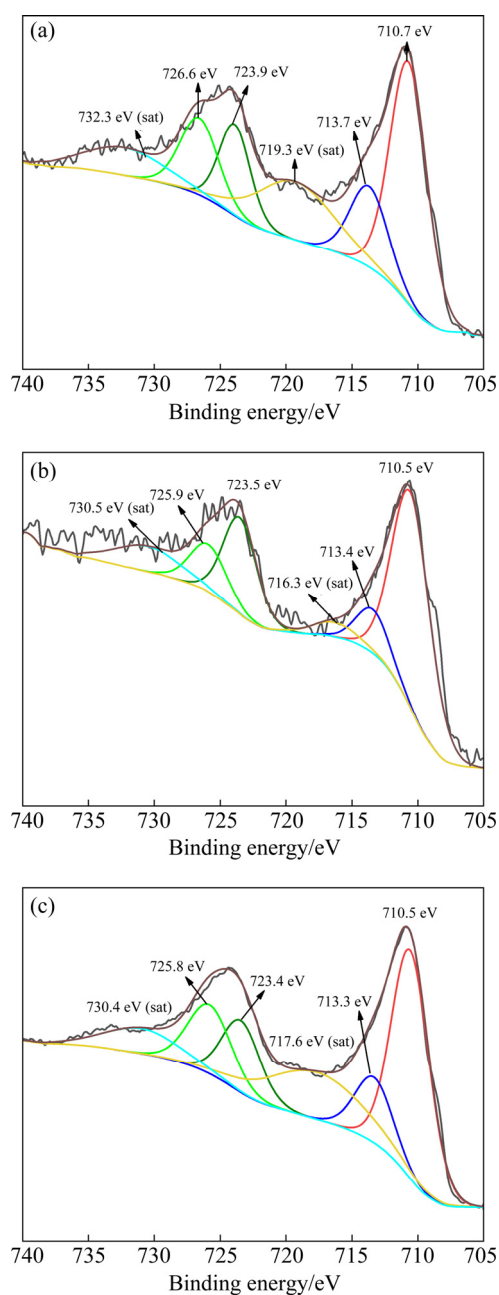


Fig. 7 XPS spectra of Fe 2p on surfaces of bare (a), SPA-treated (b) and SPE-treated ilmenite (c)

exhibited peaks at 710.7 and 713.7 eV that were assigned to Fe 2p_{3/2} of Fe²⁺ [37] and Fe³⁺ [38], respectively. In addition, two characteristic peaks at 723.9 and 726.6 eV represented the Fe 2p_{1/2} peak of iron species [39,40]. The remaining peaks at 719.3 and 732.3 eV represented the satellite peaks of iron species [41]. After treatment with SPA (Fig. 7(b)), the binding energies of Fe²⁺ and Fe³⁺ in the Fe 2p_{3/2} spectrum of ilmenite surfaces shifted by 0.2 and 0.3 eV, respectively, suggesting the chemical adsorption of SPA onto the Fe sites of the ilmenite surface. As shown in Fig. 7(c), the binding energies

of Fe²⁺ shifted by 0.2 eV and that of Fe³⁺ changed by 0.4 eV in the Fe 2p_{3/2} spectrum after the addition of SPE, indicating a stronger chemical interaction of SPE with Fe sites on the ilmenite surface.

3.4 Computational chemistry for revealing adsorption mechanism

3.4.1 Frontier orbital theory analysis for SPA/SPE molecules

The frontier orbital theory plays a significant role in describing the reactivity of molecules, where the molecular electrostatic potential (MEP) predicts the active sites of molecules [42], the lowest unoccupied molecule orbital (LUMO) reflects the electron-accepting ability, and the highest occupied molecule orbital (HOMO) reflects the electron-donating ability [43,44].

The MEP map is a useful tool for visualizing electrostatic potential regions through color grading [45]. MEP maps of SPA and SPE are calculated and shown in Fig. 8. During the SPA and SPE structure optimization, LDA-PWC was used for the exchange relation potential. The orbital cutoff quality and SCF tolerance were selected as the medium. The most negative and positive electrostatic potential regions are marked in red and blue, respectively. The map colors change from -1.63 eV (darkest red) to 1.63 eV (darkest blue). The negative charges of both collectors are mainly concentrated on the benzene ring and oxygen atoms, indicating that the benzene ring and oxygen atoms are the electron-donating centers. However, the weak electron-donating ability of the benzene ring revealed that the oxygen atom should be the main electron-donating center. The results show that SPE has a greater electron-donating ability than SPA

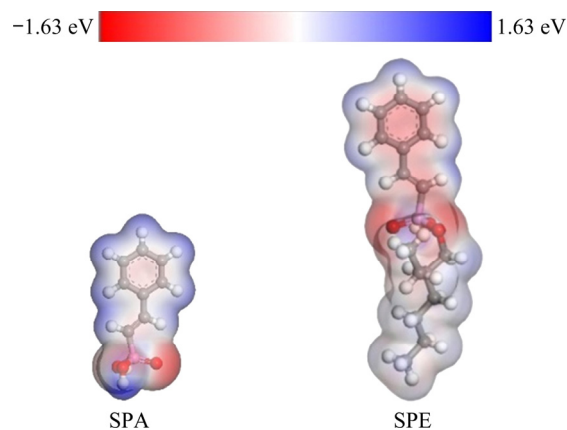


Fig. 8 MEP maps of SPA and SPE

because the oxygen atoms of the P=O and —OH groups in SPE molecules have more negative charges than those in SPA [12].

The HOMO and LUMO of SPA and SPE are shown in Fig. 9. Figures 9(a) and (b) show that the HOMO orbits are mainly centered on the benzene ring, and the C=C group is partially on the ketonic oxygen of the P=O group. Although the distribution of LUMO orbits is not much different from that of HOMO, it has fewer orbits on the P=O group. The orbital distribution implies the transfer of the electron density from the HOMO of the P=O group to the low-lying LUMO of the benzene ring.

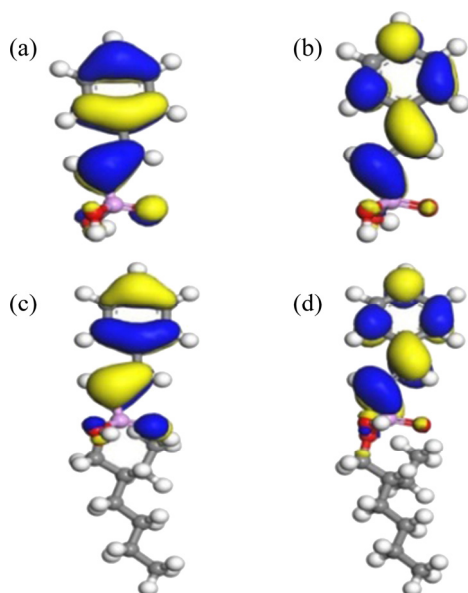


Fig. 9 Electron cloud pictures of frontier molecular orbitals of optimized collector models: (a) HOMO of SPA; (b) LUMO of SPA; (c) HOMO of SPE; (d) LUMO of SPE

The HOMO and LUMO compositions of SPA and SPE are displayed in Fig. 9, demonstrating that the benzene ring, O atoms and C=C group in the SPA molecule are the main contributors to its LUMO. The LUMO of SPE is also composed of the benzene ring, O atoms and C=C group, while the electron transfer is more obvious, indicating that SPE has a stronger electron-delocalization ability than SPA. SPA and SPE have HOMOs composed of a benzene ring, O atoms and a C—P group, which can be attributed to the chemically active centers of these two collectors.

The global reactivity parameters for the headline compound are calculated from E_{HOMO} and

E_{LUMO} and are shown in Table 2. The energy gap value, $E_{\text{LUMO-HOMO}}$, possesses chemical reactivity and is described as follows [46]:

$$E_{\text{LUMO-HOMO}} = E_{\text{LUMO}} - E_{\text{HOMO}} \quad (5)$$

where the E_{LUMO} and E_{HOMO} parameters were originally calculated by Hückel molecular orbital theory. As shown, the HOMO energy of SPE (−0.2232 eV) is higher than that of SPA (−0.2262 eV), confirming the stronger electron-donation ability of SPE. The energy gaps of SPA and SPE are observed to be 0.1284 and 0.1277 eV, respectively. The energy difference between the HOMO and LUMO determines the polarization rate and chemical activity of the molecule [44]; thus, SPE has higher chemical activities than SPA.

Table 2 Frontier orbital energies and energy differences of collectors

Collector	$E_{\text{HOMO}}/\text{eV}$	$E_{\text{LUMO}}/\text{eV}$	$E_{\text{LUMO-HOMO}}/\text{eV}$
SPA	−0.2262	−0.0978	0.1284
SPE	−0.2232	−0.0954	0.1277

3.4.2 DFT calculations for adsorption of SPA/SPE onto ilmenite surface

To examine the bonding nature of the chemical bonds before and after the adsorption of SPA or SPE in the ilmenite system, the partial densities of states (PDOS) for Ti are shown in Fig. 10. Before collector adsorption (Fig. 10(a)), the most relevant contribution from Ti atoms to the electronic band structure of orthorhombic ilmenite is a 3d band at −6.0 eV and a 3d band between 0 and 2.5 eV. In comparison, after the adsorption of SPA (Fig. 10(b)) and SPE (Fig. 10(c)), the PDOS peak for bonding Ti 3d is changed at the Fermi level. This result demonstrates that O atoms bond to Ti atoms, and the electron is transferred between these bonding atoms.

The PDOS of the Fe atoms onto ilmenite surface before and after SPA and after SPE adsorption are shown in Fig. 11. The Fe 3d states are distributed near the Fermi level. There are two DOS peaks located at −4.0 and −0.8 eV before collector adsorption (Fig. 11(a)). After SPA adsorption, the Fe 3d orbital peak drops down to two peaks at the energy level from −4.0 to −6.4 eV (Fig. 11(b)). This change indicates that the Fe 3d orbit of ilmenite is involved in the interaction between the Fe atoms and O atoms of SPA. After

SPE is adsorbed onto the ilmenite surface (Fig. 11(c)), the change in the PDOS of the Fe 3p orbital is much more obvious than that of SPA. These results prove that the adsorption of SPE can enhance the chemical reactivity of the ilmenite surface more effectively than SPA. The changes in PDOS for the Fe atom on the ilmenite surface are larger than those of the Ti atom, which is consistent with the XPS analysis results.

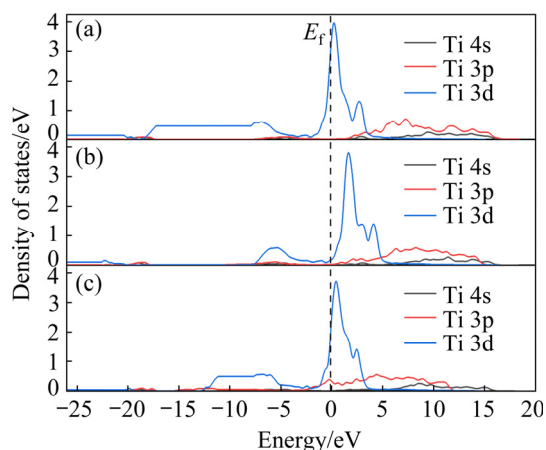


Fig. 10 PDOS of bonding Ti atoms for (104) ilmenite surface: (a, b) Before and after SPA adsorption, respectively; (c) After SPE adsorption

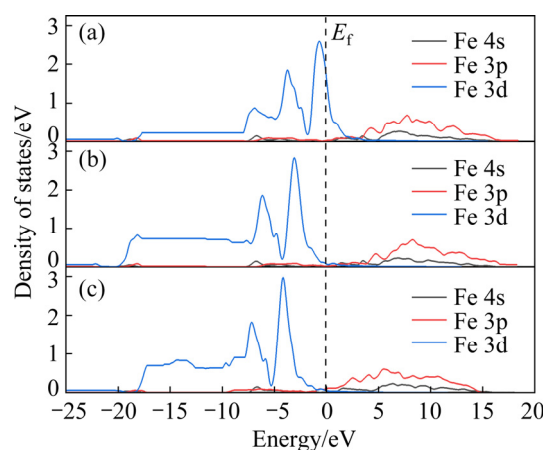


Fig. 11 PDOS of bonding Fe atoms for (104) ilmenite surface: (a, b) Before and after SPA adsorption, respectively; (c) After SPE adsorption

3.4.3 Bonding models between SPA/SPE and hematite surface

Based on the XPS analysis and the frontier orbital theory, it can be concluded that SPA and SPE interact mainly with the PO—H group of ilmenite to generate the PO—Fe and PO—Ti structures. The bonding model of collectors on the ilmenite surface is shown in Fig. 12. The calculated

adsorption energy values are listed in Table 3. As shown, SPA and SPE can chelate with ilmenite to generate a four-membered ring through the PO—Fe or PO—Ti bond. Meanwhile, the calculation results reveal that the binding energies of SPA and SPE onto the ilmenite surface are -312.46 and -359.89 kJ/mol, respectively. This indicates that SPA and SPE can easily interact with the ilmenite surface since both of these binding energies are largely negative. Additionally, Table 3 also shows that the adsorption energy of SPE onto the ilmenite surface is more negative than that of SPA, suggesting that SPE exhibits higher reaction activity to ilmenite than SPA. All these calculation results demonstrate that the adsorption of SPE onto the ilmenite surface is a chemisorption process, and SPE has a better ability to collect ilmenite than SPA.

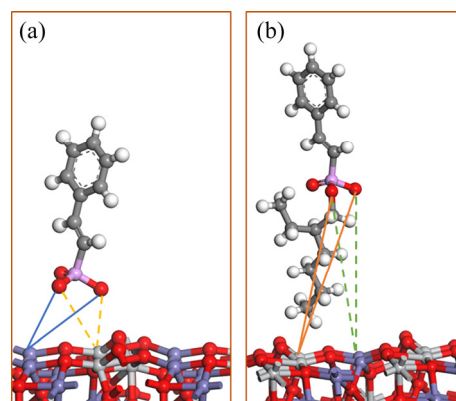


Fig. 12 Adsorption configurations of SPA (a) and SPE (b) onto (104) ilmenite surface

Table 3 Interaction energies of reagents onto (104) ilmenite surface

Sample	Adsorption energy/(kJ·mol ⁻¹)
SPA + ilmenite surface	-312.46
SPE + ilmenite surface	-359.89

4 Conclusions

(1) A novel collector, styryl phosphonate ester (SPE), was applied for ilmenite flotation and compared with the traditional collector SPA. The results of microflotation tests revealed that SPE had a stronger collecting ability to ilmenite during flotation than SPA. The application of SPE for ilmenite flotation could greatly reduce the collector concentration and has the potential to replace SPA in practice.

(2) Zeta potential measurements found that the zeta potential of ilmenite surface negatively shifted after the addition of SPE and SPA, while SPE had more significant effects than SPA, suggesting the stronger adsorption of SPE on the ilmenite surface. XPS analysis indicated that SPA and SPE could interact with the Fe and Ti atoms of the ilmenite surface by chemical bonding.

(3) Frontier orbital theory was used to predict the structure–reactivity relationship of SPE and SPA molecules, revealing that the reactive sites of SPE molecules were mainly located on the P=O and —OH groups. Therefore, SPE possessed a stronger ability to donate electrons to ilmenite than SPA. PDOS modeling demonstrated that the adsorption of SPE could improve the chemical reactivity of the ilmenite surface more obviously than the adsorption of SPA. The adsorption of collectors onto the ilmenite surface occurred by interacting the PO—H groups of the collectors with the Fe/Ti atoms of the ilmenite surface.

(4) DFT calculations also indicated that both SPA and SPE could interact with Fe and Ti atoms to generate a stable four-member ring on the ilmenite surface, while SPE (−359.89 kJ/mol) showed a higher adsorption energy than SPA (−312.46 kJ/mol) on the (104) ilmenite surface.

Supplementary Materials

Supplementary Materials in this work can be found at: http://tnmsc.csu.edu.cn/download/19-p4088-2021-1175-Supplementary_Materials.pdf.

Acknowledgments

The authors acknowledge the support from the National Natural Science Foundation of China (Nos. 51904214 and 51804238), the Young Elite Scientists Sponsorship Program by CAST (No. YESS20200276), the Natural Science Foundation of Hubei Province, China (No. ZRMS2021000085), the Fundamental Research Funds for the Central Universities, China (No. 2021IVA039), the Open Foundation of State Key Laboratory of Mineral Processing, BGRIMM Technology, China (Nos. BGRIMM-KJSKL-2021-22 and BGRIMM-KJSKL-2022-02), and the Open Project of Engineering Research Center of Phosphorus Resources Development and Utilization of Ministry of Education, China (No. 201904).

References

- [1] DU Yu-sheng, MENG Qing-you, YUAN Zhi-tao, MA Long-qiu, ZHAO Xuan, XU Yuan-kai. Study on the flotation behavior and mechanism of ilmenite and titanite with sodium oleate [J]. *Minerals Engineering*, 2020, 152(1): 106366.
- [2] MEHDILO A, IRANNAJAD M, REZAI B. Effect of chemical composition and crystal chemistry on the zeta potential of ilmenite [J]. *Colloids and Surfaces A: Physicochemical and Engineering Aspects*, 2013, 428: 111–119.
- [3] ZHAI Ji-hua, CHEN Pan, WANG Hong-bin, HU Yue-hua, SUN Wei. Flotability improvement of ilmenite using attrition-scrubbing as a pretreatment method [J]. *Minerals*, 2017, 7(1): 13.
- [4] CHEN Hang, MI Guang-bao, LI Pei-jie, HUANG Xu, CAO Chun-xiao. Extremely high beta-transus temperature of graphene oxide reinforced high-temperature titanium alloy matrix composite [J]. *Materials Letters*, 2021, 291(7): 129575.
- [5] ZHAI Ji-hua, CHEN Pan, SUN Wei, CHEN Wei, WAN Si. A review of mineral processing of ilmenite by flotation [J]. *Minerals Engineering*, 2020, 157: 106558.
- [6] LIU Wei-jun, ZHANG Jie, WANG Wei-qing, DENG Jie, CHEN Bing-yan, YAN Wu, XIONG Shu-qing, HUANG Yang, LIU Jing. Flotation behaviors of ilmenite, titanite, and forsterite using sodium oleate as the collector [J]. *Minerals Engineering*, 2015, 72: 1–9.
- [7] ZHAO Xuan, MENG Qing-you, YUAN Zhi-tao, ZHANG Yun-hai, LI Li-xia. Effect of sodium silicate on the magnetic separation of ilmenite from titanite by magnetite selective coating [J]. *Powder Technology*, 2019, 344: 233–241.
- [8] FARJANA S H, HUDA N, MAHMUD M A P, LANG C. Towards sustainable TiO₂ production: An investigation of environmental impacts of ilmenite and rutile processing routes in Australia [J]. *Journal of Cleaner Production*, 2018, 196: 1016–1025.
- [9] MEHDILO A, IRANNAJAD M, REZAI B. Chemical and mineralogical composition of ilmenite: Effects on physical and surface properties [J]. *Minerals Engineering*, 2015, 70: 64–76.
- [10] ZHAI Ji-hua, LU Xiao-long, CHEN Pan, GUAN Chang-ping, SUN Wei, CHEN Wei. A new collector scheme for strengthening ilmenite floatability in acidic pulp [J]. *Journal of Materials Research and Technology*, 2019, 8(5): 5053–5056.
- [11] YANG Yao-hui, XU Long-hua, LIU Ya-chuan, HAN Yue-xin. Flotation separation of ilmenite from titanite using mixed collectors [J]. *Separation Science and Technology*, 2016, 51(11): 1840–1846.
- [12] HUANG Kai-hua, HUANG Xiao-ping, JIA Yun, WANG Shuai, CAO Zhan-fang, ZHONG Hong. A novel surfactant styryl phosphonate mono-iso-octyl ester with improved adsorption capacity and hydrophobicity for cassiterite flotation [J]. *Minerals Engineering*, 2019, 142: 105895.
- [13] YANG Zhi-ren, BIAN Xue, WU Wen-yuan. Flotation

- performance and adsorption mechanism of styrene phosphonic acid as a collector to synthetic (Ce,La)₂O₃ [J]. *Journal of Rare Earths*, 2017, 35(6): 621–628.
- [14] LI Li-xia, ZHANG Chen, YUAN Zhi-tao, LIU Zhi-chao, LI Chun-feng. Selectivity of benzyl hydroxamic acid in the flotation of ilmenite [J]. *Frontiers in Chemistry*, 2019, 7: 886.
- [15] FANG Shuai, XU Long-hua, WU Hou-qin, SHU Kai-qian, XU Yan-bo, ZHANG Zhen-yue, CHI Ruan, SUN Wei. Comparative studies of flotation and adsorption of Pb(II)/benzohydroxamic acid collector complexes on ilmenite and titanite [J]. *Powder Technology*, 2019, 345: 35–42.
- [16] YANG Si-yuan, QIU Xian-yang, PENG Tie-feng, CHANG Zi-yong, FENG Qi-ming. Beneficial effects and mechanism of lead ion on wolframite flotation [J]. *Physicochemical Problems of Mineral Processing*, 2016, 52(2): 855–873.
- [17] YANG Si-yuan, PENG Tie-feng, LI Hong-qiang, FENG Qi-ming, QIU Xian-yang. Flotation mechanism of wolframite with varied components Fe/Mn [J]. *Mineral Processing and Extractive Metallurgy Review*, 2015, 37(1): 1104505.
- [18] LIU Cheng, ZHU Yu-hua, HUANG Kai-hua, YANG Si-yuan, LIANG Zhi-an. Studies of benzyl hydroxamic acid/calcium lignosulphonate addition order in the flotation separation of smithsonite from calcite [J]. *International Journal of Mining Science and Technology*, 2021, 31(6): 1153–1158.
- [19] GRUNER H, BILSING U. Cassiterite flotation using styrene phosphonic acid to produce high-grade concentrates at high recoveries from finely disseminated ores—Comparison with other collectors and discussion of effective circuit configurations [J]. *Minerals Engineering*, 1992, 5(3): 429–434.
- [20] LI Fang-xu, ZHONG Hong, ZHAO Gang, WANG Shuai, LIU Guang-yi. Flotation performances and adsorption mechanism of α -hydroxyoctyl phosphinic acid to cassiterite [J]. *Applied Surface Science*, 2015, 353: 856–864.
- [21] TAN Xin, HE Fa-yu, SHANG Yan-bo, YIN Wan-zhong. Flotation behavior and adsorption mechanism of (1-hydroxy-2-methyl-2-octenyl) phosphonic acid to cassiterite [J]. *Transactions of Nonferrous Metals Society of China*, 2016, 26(9): 2469–2478.
- [22] LI Fang-xu, ZHOU Xiao-tong, LIN Ri-xiao. Flotation performance and adsorption mechanism of novel 1-(2-hydroxyphenyl)hex-2-en-1-one oxime flotation collector to malachite [J]. *Transactions of Nonferrous Metals Society of China*, 2020, 30(10): 2792–2801.
- [23] HUANG Kai-hua, CAO Zhan-fang, WANG Shuai, YANG Jia, ZHONG Hong. Flotation performance and adsorption mechanism of styryl phosphonate mono-iso-octyl ester to malachite [J]. *Colloids and Surfaces A: Physicochemical and Engineering Aspects*, 2019, 579(10): 123698.
- [24] LIU Sheng, LIU Guang-yi, HUANG Yao-guo, ZHONG Hong. Hydrophobic intensification flotation: Comparison of collector containing two minerophilic groups with conventional collectors [J]. *Transactions of Nonferrous Metals Society of China*, 2020, 30(9): 2536–2546.
- [25] CHEN Bo, BAO Shen-xu, ZHANG Yi-min. Synergetic strengthening mechanism of ultrasound combined with calcium fluoride towards vanadium extraction from low-grade vanadium-bearing shale [J]. *International Journal of Mining Science and Technology*, 2021, 31(6): 1095–1106.
- [26] BAI Shao-jun, YU Pan, DING Zhan, BI Yun-xiao, LI Chun-long, WU Dan-dan, WEN Shu-ming. New insights into lead ions activation for microfine particle ilmenite flotation in sulfuric acid system: Visual MINTEQ models, XPS, and ToF–SIMS studies [J]. *Minerals Engineering*, 2020, 155: 106473.
- [27] AI Guang-hua, HUANG Kai-hua, LIU Cheng, YANG Si-yuan. Exploration of amino trimethylene phosphonic acid to eliminate the adverse effect of seawater in molybdenite flotation [J]. *International Journal of Mining Science and Technology*, 2021, 31(6): 1129–1134.
- [28] ARAUJO C, FREIRE C S R, NOLASCO M M, RIBEIRO-CLARO P J A, RUDIĆ S, SILVESTRE A J D, VAZ P D. Hydrogen bond dynamics of cellulose through inelastic neutron scattering spectroscopy [J]. *Biomacromolecules*, 2018, 19(4): 1305–1313.
- [29] SILVEIRA J E, PAZ W S, GARCIA-MUÑOZ P, ZAZO J A, CASAS J A. UV-LED/ilmenite/persulfate for azo dye mineralization: The role of sulfate in the catalyst deactivation [J]. *Applied Catalysis B: Environmental*, 2017, 219: 314–321.
- [30] CHETTAB M, SIMON Q, ZAGHRIQUI M, AUTRET-LAMBERT C, LAFPEZ P. Influence of sputtering conditions and annealing parameters on structure and morphology of NiTiO₃ ilmenite thin films [J]. *Thin Solid Films*, 2020, 714: 138384.
- [31] ZHU Guang-li, CAO Yi-jun, WANG Yu-hua, WANG Xu-ming, MILLER J D, LU Dong-fang, ZHENG Xia-yu. Surface chemistry features of spodumene with isomorphous substitution [J]. *Minerals Engineering*, 2020, 146: 106139.
- [32] CHEN Pan, LU Xiao-long, CHAI Xu-jian, MULENGA H, GAO Jian-de, LIU Hang, MENG Qing-bo, SUN Wei, GAO Yu-de. Influence of Fe–BHA complexes on the flotation behavior of ilmenite [J]. *Colloids and Surfaces A: Physicochemical and Engineering Aspects*, 2021, 612: 125964.
- [33] LUO Li-ping, WU Hou-qin, YANG Jie, TANG Zhen, SHU Kai-qian, XU Yan-bo, YAN Wei-pin, XU Long-hua. Effects of microwave pre-treatment on the flotation of ilmenite and titanite [J]. *Minerals Engineering*, 2020, 155(8): 106452.
- [34] MIAO Chun-hui, SHI Tong-fei, XU Guo-ping, JI Shu-lin, YE Chang-hui. Photocurrent enhancement for Ti-doped Fe₂O₃ thin film photoanodes by an in situ solid-state reaction method [J]. *ACS Applied Materials & Interfaces*, 2013, 5(4): 1310–1316.
- [35] PHOONKONG W, PAVASUPREE S, WANNAGON A, BOONYARATTANAKALIN K, MEKPRASART W, PECHARAPA W. Electrochemical properties of nanopowders derived from ilmenite and leucocene natural minerals [J]. *Ceramics International*, 2017, 43(Supplement 1): S717–S722.
- [36] SANTARA B, GIRI P K, DHARA S, IMAKITA K, FUJII M. Oxygen vacancy mediated enhanced ferromagnetism in undoped and Fe doped TiO₂ nanoribbons [J]. *Journal of Physics D: Applied Physics*, 2014, 47(23): 235304.
- [37] BONNISSEL-GISSINGER P, ALNOT M, EHRHARDT J J, BEHRA P. Surface oxidation of pyrite as a function of pH [J].

- Environmental Science & Technology, 1998, 32(19): 2839–2845.
- [38] BRION D. Study by photoelectron-spectroscopy of surface degradation of FeS₂, CuFeS₂ ZnS and PbS exposed to air and water [J]. Applications of Surface Science, 1980, 5(2): 133–152.
- [39] CAI Jiao-zhong, DENG Jiu-shuai, WEN Shu-ming, ZHANG Ying, WU Dan-dan, LUO Hong-ying, CHENG Gan. Surface modification and flotation improvement of ilmenite by using sodium hypochlorite as oxidant and activator [J]. Journal of Materials Research and Technology, 2020, 9(3): 3368–3377.
- [40] YUAN Shuai, WANG Ruo-feng, GAO Peng, HAN Yue-xin, LI Yan-jun. Suspension magnetization roasting on waste ferromanganese ore: A semi-industrial test for efficient recycling of value minerals [J]. Powder Technology, 2022, 396: 80–91.
- [41] HAMILTON T, HUAI Yang-yang, PLACKOWSKI C, PENG Yong-jun. The interactions of radioactive lead with sulphide minerals [J]. Applied Surface Science, 2021, 538: 148141.
- [42] BARIM E, AKMAN F. Synthesis, characterization and spectroscopic investigation of N-(2-acetylbenzofuran-3-yl) acrylamide monomer: Molecular structure, HOMO–LUMO study, TD-DFT and MEP analysis [J]. Journal of Molecular Structure, 2019, 1195: 506–513.
- [43] ARASU N, ASIRVATHAM P, PRIYA M K, REVATHI B K. Spectroscopic (FT-IR, Raman, ¹³C and ¹H NMR) investigation, molecular orbital calculation and thermal properties of novel piperidine derivative compound by quantum chemical calculation [J]. Materials Today: Proceedings, 2019, 8: 47–56.
- [44] FAZILATH BASHA A, KHAN F L A, MUTHU S, RAJA M. Computational evaluation on molecular structure (Monomer, dimer), RDG, ELF, electronic (HOMO–LUMO, MEP) properties, and spectroscopic profiling of 8-quinolinesulfonamide with molecular docking studies [J]. Computational and Theoretical Chemistry, 2021, 1198: 113169.
- [45] LU Yu-xi, WANG Shuai, ZHONG Hong. Study on the role of a hydroxamic acid derivative in wolframite flotation: Selective separation and adsorption mechanism [J]. Applied Surface Science, 2021, 550: 149223.
- [46] KOKALJ A. On the alleged importance of the molecular electron-donating ability and the HOMO–LUMO gap in corrosion inhibition studies [J]. Corrosion Science, 2021, 180: 109016.

捕收剂苯乙烯膦酸酯在钛铁矿浮选中的吸附机理

徐艳玲¹, 黄凯华², 李洪强³, 黄伟⁴, 刘诚¹, 杨思原^{1,3}

1. 武汉理工大学 资源与环境工程学院, 武汉 430070;
2. 中国生态环境部 华南环境科学研究所, 广州 510530;
3. 武汉工程大学 磷资源开发利用教育部工程研究中心, 武汉 430205;
4. 南方科技大学 前沿与交叉科学研究院, 深圳 518055

摘要: 采用捕收剂苯乙烯膦酸酯(SPE)提高钛铁矿浮选效率, 揭示相关作用机理并建立吸附模型。单矿物浮选试验结果表明, SPE 在钛铁矿浮选中表现出比传统苯乙烯膦酸(SPA)更强的捕收能力。Zeta 电位测定结果显示, SPE 和 SPA 都能使钛铁矿的 Zeta 电位负向移动, 而 SPE 的作用效果比 SPA 更加明显, 表明 SPE 在钛铁矿表面的吸附更强。X 射线光电子能谱分析证实了 SPA 和 SPE 在钛铁矿的 Fe/Ti 位点上的化学吸附作用。前沿轨道理论分析结果表明, SPE 的化学活性比 SPA 的高。局部态密度分析结果表明, 两种捕收剂的 PO—H 基团可与钛铁矿的 Ti/Fe 原子相互作用, 从而在钛铁矿表面生成一个稳定的四元环。捕收剂与(104)钛铁矿表面的结合模型显示, SPE 的吸附能量高于 SPA 的。综上所述, SPE 对钛铁矿浮选的捕收能力和作用效果均优于 SPA 的, 具有在工业上替代 SPA 的潜力。

关键词: 苯乙烯膦酸酯; 钛铁矿; 浮选; 捕收剂; X 射线光电子能谱; 密度泛函理论; 吸附机理

(Edited by Wei-ping CHEN)